Journal of Biomedical Optics

SPIEDigitalLibrary.org/jbo

Noninvasive monitoring of gas in the lungs and intestines of newborn infants using diode lasers: feasibility study

Patrik Lundin
Emilie Krite Svanberg
Lorenzo Cocola
Märta Lewander Xu
Gabriel Somesfalean
Stefan Andersson-Engels
John Jahr
Vineta Fellman
Katarina Svanberg
Sune Svanberg

SPIE

Noninvasive monitoring of gas in the lungs and intestines of newborn infants using diode lasers: feasibility study

Patrik Lundin,[a,*,†] Emilie Krite Svanberg,[b,c,†] Lorenzo Cocola,[a,d] Märta Lewander Xu,[e] Gabriel Somesfalean,[a] Stefan Andersson-Engels,[a] John Jahr,[b] Vineta Fellman,[f] Katarina Svanberg,[g,h] and Sune Svanberg[a,h]
[a]Lund University, Department of Physics, P.O. Box 118, SE-221 00 Lund, Sweden
[b]Lund University, Skåne University Hospital, Department of Anesthesiology and Intensive Care Medicine, SE-221 85 Lund, Sweden
[c]Lund University, Skåne University Hospital, Department of Anesthesiology and Intensive Care Medicine, SE-205 02 Malmö, Sweden
[d]CNR Institute for Photonics and Nanotechnologies–LUXOR, Via Trasea 7, IT-351 31 Padova, Italy
[e]Gasporox AB, Magistratsvägen 10, SE-226 43 Lund, Sweden
[f]Lund University, Department of Pediatrics, SE-221 85 Lund, Sweden
[g]Lund University, Department of Oncology, SE-221 85 Lund, Sweden
[h]South China Normal University, Center for Optical and Electromagnetic Research, Guangzhou CN-510006, China

Abstract. Preterm newborn infants have a high morbidity rate. The most frequently affected organs where free gas is involved are the lungs and intestines. In respiratory distress syndrome, both hyperexpanded and *atelectatic* (collapsed) areas occur, and in necrotizing enterocolitis, intramural gas may appear in the intestine. Today, these conditions are diagnosed with x-ray radiography. A bed-side, rapid, nonintrusive, and gas-specific technique for *in vivo* gas sensing would improve diagnosis. We report the use of noninvasive laser spectroscopy, for the first time, to assess gas content in the lungs and intestines of three full-term infants. Water vapor and oxygen were studied with two low-power diode lasers, illuminating the skin and detecting light a few centimeters away. Water vapor was easily detected in the intestines and was also observed in the lungs. The relatively thick chest walls of the infants prevented detection of the weaker oxygen signal in this study. However, results from a previous phantom study, together with scaling of the results presented here to the typical chest-wall thickness of preterm infants, suggest that oxygen also should be detectable in their lungs. [DOI: 10.1117/1.JBO.18.12.127005]

Keywords: diode laser; spectroscopy; oxygen; water vapor; lungs; respiratory distress syndrome; surfactant; gastrointestinal tract; necrotizing enterocolitis.

Paper 130694PR received Sep. 23, 2013; revised manuscript received Nov. 21, 2013; accepted for publication Nov. 22, 2013; published online Dec. 20, 2013.

1 Introduction

In Europe and the United States, ~6 to 15% of deliveries are preterm (delivered before gestation week 37),[1] and are associated with increased risk of morbidities because of immature organs. Respiratory distress syndrome (RDS) is a lung disease affecting preterm infants during the first days of life,[2] which is caused by an insufficiency of surfactant (alveoli coating protein, preventing their collapse) and structurally immature lung. Chest radiographs show a reticulogranular pattern, which is thought to represent an inhomogeneous lung aeration with multiple small air spaces being fluid-filled or collapsed.[3] The prevalence of RDS is ~1% of all newborn infants, with increasing incidence with decreasing gestational age. About 50% of infants born in gestation weeks 26 to 28, and ~25% of those born in weeks 30 to 31, are affected. It may result in a typical chronic lung disease of prematurity, bronchopulmonary dysplasia.

The most common gastrointestinal emergency affecting preterms is necrotizing enterocolitis (NEC),[4] an acute inflammatory disease in which portions of the intestine undergo necrosis (tissue death) with a risk of intestinal perforation, associated with high morbidity and mortality rates. The incidence of NEC ranges from 1 to 8%, with 90% of all NEC cases occurring among very preterm infants. Initial symptoms include intolerance to feeding, abdominal distension (due to increased amount of gas in the intestine), increased gastric residuals, and bloody stools. As the disease progresses, intramural (in the intestinal wall) gas accumulates.

Even though preterm infants undergoing intensive care are continuously monitored with sophisticated equipment, the severity of the disease is difficult to assess. The diagnostic method for assessing infant lungs is mainly ionizing radiation-based scanning, and repeated exposure to this highly energetic radiation can be associated with harmful health effects. Electrical impedance tomography can give a two-dimensional view of lung aeration,[5] but the technique is not commercially available for small infants. Effect of adjustment in ventilator treatment is mainly assessed clinically with the help of venous and arterial blood gases.

The initial suspicion of NEC is based on clinical findings and an x ray showing intramural and intrahepatic (inside the liver) gas, dilated bowel loops, paucity of gas (unaltered gas-filled loop of bowel), and pneumoperitoneum (air outside the bowel within the abdomen). Ultrasound is a noninvasive

[†]These authors contributed equally to the work and should be considered as co-first authors.

*Address all correspondence to: Patrik Lundin, E-mail: patrik.lundin@fysik.lth.se

0091-3286/2013/$25.00

technique used to visualize different types of tissue and air-filled spaces within the body. However, the constituents of the gas (e.g., oxygen, nitrogen, or carbon dioxide) cannot be obtained with the presently available techniques.

Disease severity, especially the development of pneumothorax (collapsed lung) and free gas in the abdomen, as well as assessment of ventilation efficacy would be improved with a technique showing the spatial gas distribution and gas constituents within the thoracal and abdominal cavities. As a first step toward applying noninvasive techniques, Lewander et al. carried out a feasibility study with a laser technique on phantoms built up as the superior thoracal aperture of a preterm infant.[6] These phantoms were made up of animal (wild boar) lung tissue covered by gelatin layers with scattering particles and absorbing ink, mimicking the chest wall of a small infant. Oxygen and water vapor could readily be detected, a result encouraging the next natural step—*in vivo* measurements.

The present paper presents the first *in vivo* measurements with a laser spectroscopic technique for detection of gas in the lungs and intestines of three full-term infants. The optically based technique uses laser light tuned to be absorbed by water vapor and oxygen gas. The recently developed method is named gas in scattering media absorption spectroscopy (GASMAS)[7] and it is a variety of tunable diode laser absorption spectroscopy. With this method, it is possible to detect the sharp absorption imprints derived from free gas, even when surrounded by a strongly scattering medium, such as the human tissue. The study is a step toward developing a method to monitor gas in preterm infants. An early account of the study is given in Ref. 8.

2 Principles

2.1 *Tissue Optics*

Tissue, being mainly composed of water, blood, fat, proteins, and skeletal structures, exhibits the tissue optical window ranging from wavelengths of ~600 nm to 1.3 μm, in which the light absorption is relatively weak so that light can be reasonably well transmitted although the light scattering is still strong.[9] The lower wavelength limit is due to the absorption of hemoglobin and oxyhemoglobin,[10] while the upper one is mainly due to (liquid) water absorption.[11] In this window, the tissue has optical properties so that, on average, the light traveling in the tissue will change direction completely ~10 times per centimeter (reduced scattering coefficient, $\mu_s' \approx 10\ \mathrm{cm}^{-1}$), while ~10 to 40% of the light is absorbed after every centimeter of travel (absorption coefficient, $\mu_a \approx 0.1$ to $0.4\ \mathrm{cm}^{-1}$). When illuminating tissue in this spectral region, it is thus possible to detect diffuse light some distance away on the same surface or on the other side of an object. The path-length that the light has traveled between the position of the source and detector is greatly prolonged due to the scattering.

A major challenge in the field of tissue optics is to understand the light propagation on a detailed level, following light injected into the tissue. Furthermore, it is demanding to calculate the photon-hitting density, i.e., the spatial distribution of the conditional occupancy for light injected in the tissue at one position and detected at another. One way to obtain some information on this, when analytical approaches are difficult or impossible to apply, is to perform Monte Carlo simulations. This type of simulation is used for describing the light propagation in the present paper.

2.2 *Principle of the Spectroscopic Technique*

Gas present in pores or cavities embedded in the tissue will create sharp and species-unique absorption imprints in the transmitted light, which are readily observed in the detected signal. The measurement technique GASMAS (Ref. 7) is utilizing these gas absorption features and has earlier been shown to perform well for gas assessment in human sinus cavities for diagnosis of sinusitis[12–15] and in the mastoid bone,[16] as well as in many non-biological light scattering objects, e.g., wood,[17] pharmaceutical tablets,[18,19] ceramics,[20] food packages,[21,22] fruits,[23,24] etc. In short, the technique can be used to evaluate the gas content of small pores or larger cavities embedded in strongly scattering (turbid) media. In this study, the gases of interest are oxygen (O_2) and water vapor (H_2O), which have a number of absorption lines at light wavelengths around 760 and 935 nm, respectively.

In order to probe a gas, a tunable laser is scanned across a wavelength interval where the gas of interest has an absorption line and the light is sent through a path with the gas. A detector records the intensity of the light that has passed though the gas as a function of time. At the time of the scan when the laser wavelength exactly matches the wavelength of the absorption line, a slightly lower intensity is recorded [see Fig. 1(a)]. The fraction of light lost at the absorption line, A, is dependent on the concentration, c, of the gas and the length of the path that the light goes through the gas, L (the path-length). This relationship is given by the Beer-Lambert law.

$$A = 1 - I/I_0 = 1 - \exp(-\varepsilon c L). \tag{1}$$

Here, I is the intensity of light recorded at the absorption line, I_0 is the intensity at wavelengths adjacent to the line, and ε is the molar extinction coefficient. Thus, by observing the magnitude

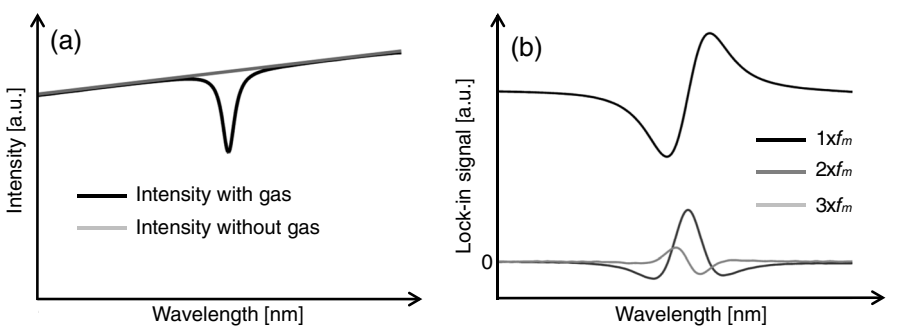

Fig. 1 Principle of tunable diode laser absorption spectroscopy and wavelength modulation spectroscopy (WMS).

of the absorption dip caused by the absorption of the gas, the product of concentration and path-length can be found (the extinction coefficient is constant and well known). To extract the concentration or path-length from their product, the other factor must be known. This is further discussed in Sec. 3.2.

The performance of the detection can be improved by employing the wavelength modulation spectroscopy (WMS) technique. Basically, the wavelength of the laser is quickly modulated at a frequency f_m at the same time as it is scanned across the absorption line. By doing this, it is possible to use powerful lock-in detection approaches. A lock-in amplifier is tuned to the frequency of the modulation, as well as to overtones of this [$1 \times f_m, 2 \times f_m, 3 \times f_m, \ldots$, see Fig. 1(b)]. WMS was employed in this study in a digital manner described thoroughly in Refs. 14 and 25.

3 Materials and Subjects

3.1 *Subjects of the Case Study*

The present work is a pilot study for a project with ethical approval (no. 213–356) by the Regional Human Ethics Committee at Lund University, Sweden. Measurements were performed on three healthy, full-term infants with parental informed consent and presence at the measurements. Relevant data for the subjects are presented in Table 1.

3.2 *Technical System*

The system used for the spectroscopic study is presented in Fig. 2. Driving voltages consisting of a triangular ramp (scan) with a frequency of 5 Hz, and a superpositioned fast modulation at 9015 and 10,295 Hz for water vapor and oxygen, respectively, are generated by a LabView interface in a standard PC and sent via a data acquisition (DAQ) card (NI-6120 with connector block BNC-2110) to the laser current and temperature controllers (Thorlabs, New Jersey LCD201C and Thorlabs TED200C) controlling the drive current and temperature of the laser for water vapor analysis, respectively, and to a Melles Griot 06DLD103 unit, controlling both current and temperature of the laser for oxygen analysis. One of the lasers (Nanoplus, Gerbrunn, Germany DFB 213/6-24) emits light with a wavelength of ~760 nm, suitable to probe oxygen, while the other laser (Nanoplus, DFB 111/1-2) emits light with wavelength of ~935 nm, suitable to probe water vapor. The output power is ~4 mW for each of the lasers. Both lasers are fiber coupled and the light emissions from the two lasers are then merged together into a single fiber, thus containing light of both wavelengths. The light is then again split up in two fibers, one containing ~90% of the light (both wavelengths) and the other containing the remaining 10% (both wavelengths). The distal end of the fiber containing most of the light is placed on the skin of the infant and the light is delivered to the desired body area, while the smaller light fraction is sent directly to a reference detector used for signal improvement. The weak light detected by the two photodiodes (Hamamatsu, Hamamatsu, Japan S3204-08, active size 18×18 mm^2, and Hamamatsu S3590-01, active size 10×10 mm^2, for the *in vivo* and reference detectors, respectively) will generate small currents that are amplified and transformed into voltages with transimpedance amplifiers (Femto, Berlin, Germany DLPCA-200). The resulting signal voltages are then fed to the same DAQ card as was originally used to generate the inputs to the laser drivers. The voltage signals are recorded with a sampling rate of 400 kHz. The signals from each 0.2-s ramp can be averaged for an arbitrary number of times before being stored for further analysis. The lock-in procedure is digitally performed with a custom-made MATLAB® software, and the final result is a measure of the product of the path-length, L, and the gas concentration, c, mentioned in Sec. 2.2. The individual absorption signals by water vapor and oxygen are recovered by performing the digital lock-in amplification at the modulation frequencies for the two lasers, respectively. A reference recording through 1 m of air (temperature = 22°C, relative humidity = 32%) was performed in connection with the measurements and was used as a calibration to give quantitative values of the measured gas absorption. The strength of this absorption signal is recalculated as if it would have been performed in 100% relative humidity

Table 1 Subjects of the study.

	Subject 1	Subject 2	Subject 3
Gender	Male	Female	Female
Birth week	40	40	40
Birth length	53 cm	54 cm	51 cm
Birth weight	3890 g	4265 g	3970 g
Age at the time of study	19 days	19 days	36 days
Weight at the time of study	4280 g	4560 g	5000 g

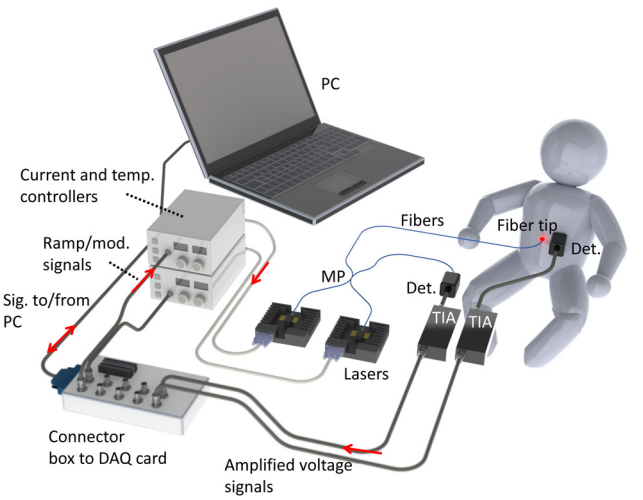

Fig. 2 Setup for the measurements. A PC with the software LabView is, through a data acquisition (DAQ) card with a connector box, sending the voltage ramp/modulation inputs to the current drivers. The current drivers are in turn sending the currents to the lasers, which emit the light into optical fibers. The light from the two lasers, being of two different wavelengths, is merged through a multiplexer (MP) and again split into two fibers (both now containing the two wavelengths). One of the fibers goes to a reference detector and one goes to the infant. The probe light is detected a small distance away from the fiber tip. The detector (Det.) converts the light to a current that is amplified and transformed to a voltage in the transimpedance amplifiers (TIA) before being sent to the connector box of the DAQ card to be sampled. The sampled voltage signals are read by the computer and stored for analysis.

and at 37°C (the *in situ* conditions) before being compared with the obtained *in situ* gas absorption signals. The absolute strength of the recorded absorption signals is then expressed in terms of equivalent mean path-length, L_{eq}, measured in units of millimeter. If the strength of the obtained absorption signal is 10% of that of a recording through 1 m of air with 100% relative humidity and a temperature of 37°C, the result is $L_{eq} =$ 100 mm. This way of expressing the result directly gives the (average) physical length that the water vapor probing light passed through gas in the body (assuming the above conditions). Assuming the light probing oxygen has the same path-length through gas[12] enables estimation of its concentration through its absorption magnitude [the only unknown remaining in Eq. (1) is c]. Due to the demanding measurement conditions with very low light transmission and small absorption imprint, the signal quality is often relatively poor. The accuracy of the final estimated gas absorption is improved by using the above calibration including a fitting procedure.

4 Methods

4.1 *Ultrasound Measurements*

Ultrasound measurements (SonoSite, Washington M-Turbo®, Linear probe, 6 to 13 MHz) were conducted on the infants to obtain images of the distance between the skin surface and the organs at interest for investigation, i.e., the thickness of the tissue surrounding the lungs and intestine, as well as the depth of possible gas pockets in the intestine. An experienced ultrasonographist performed the assessments.

The measurements on the lungs were made with the ultrasound probe placed in different positions, pointing toward the lung tissue. However, most measurements were conducted with the probe placed slightly below the collar bone [similar to the placement of the fiber in Fig. 3(a)].

For the abdominal cavity, several measurements were obtained with the ultrasound probe placed on the front side of the stomach [similar to the placement of the fiber and detector shown in Fig. 3(b)].

4.2 *Spectroscopic Lung Measurements*

The tissue surrounding the lungs of the three infants was (see Fig. 4) relatively thick and therefore difficult to penetrate with the laser light. The measurements presented in this paper therefore aimed toward trying to find a laser/detector position geometry where it was possible for the light to go deep enough to actually probe the gas in the lung and at the same time be possible to detect at another position. Numerous geometries were tested with the laser/detector at the back, chest, and side of the torso. The tissue covering the lungs is thinnest slightly below the armpit (low fat content and little muscle tissue between the skin and the ribs)—hence, it was with the detector

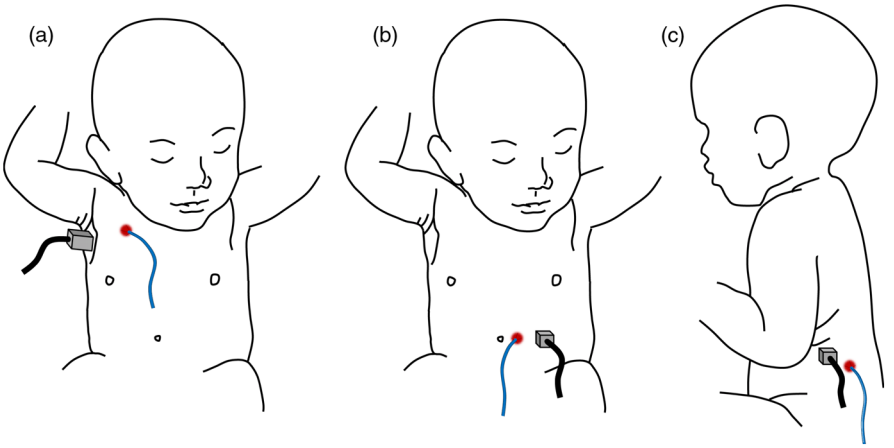

Fig. 3 (a) Geometry of the lung measurements that gave gas imprints. (b) Front geometry of the intestine measurements. (c) Back geometry of the intestine measurements. The laser light was delivered through the thin fiber and detected with the photodiode connected with a BNC cable.

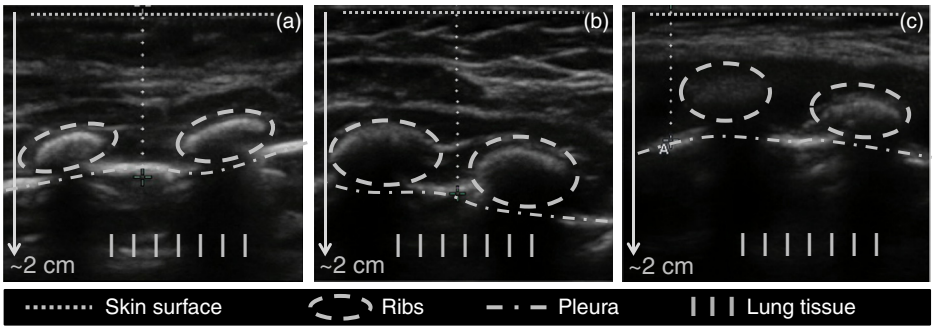

Fig. 4 Ultrasound image, showing an ~2-cm-deep thoracic wall cross-section of the three infants [(a) to (c), corresponding to subjects 1 to 3]. The probe was placed 2 cm below the right collar bone. As indicated, skin surface, ribs, pleura, and lung tissue are clearly seen.

positioned here that it was possible to detect a small absorption signal by water vapor. The geometry that was found to function best for all of the subjects is shown in Fig. 3(a), where the laser light is sent in just below the collar bone and detected through the ribcage, just below the armpit. This geometry was used on the right side of the body, sending light through the right lung.

4.3 *Spectroscopic Intestine Measurements*

Several different positions for placing the fiber tip and the detector were tested to search for any sign of oxygen or water vapor. Oxygen was not expected to be present, but if any gas-filled volumes were forthcoming, water vapor should definitely be a part of the gas. When one such source-detector configuration was found in the case of subject 1, a special study was performed where the strength of the absorption signal by water vapor was evaluated at four different fiber-to-detector separations: 20, 31, 43, and 54 mm (fiber tip to center of detector). In this geometry, shown in Fig. 3(b), the fiber probe (delivering the laser light) was positioned roughly at the height of the umbilicus and the detector was placed on the abdomen to the side of the fiber probe (at the four different separation distances). For subject 2, measurements were performed in the geometries shown in Figs. 3(b) and 3(c), while only geometry "b" was used for subject 3.

4.4 *Simulations*

Simulations were used to investigate the light transport in relation to the measurements where the fiber-detector distance was increased stepwise for the intestine measurements on subject 1. The simulations utilized a custom-made Monte Carlo program injecting single photons (i.e., not weighted photon packages) into a two-dimensional grid consisting of 200×400 blocks (depth $\times$ horizontal direction). The grid was 4 cm in depth and 10 cm in the horizontal direction. The length of each photon step was randomized in a logarithmic distribution with center-of-mass length $\langle l \rangle = 1/\mu_s' = 0.1$ cm, and the direction was completely random in 360 deg. For each step, the probability of absorption was $\mu_a \times l$, with $\mu_a = 2.5$ cm^{-1}. When 200,000 photons had reached the detector, the simulation was stopped and the paths of these photons were stored (the number of photons injected depends on the position of the detector, but, in general, hundreds of millions of photons were needed). General references for the simulation technique in the tissue optics field can be found in Refs. 26, 27, and 28.

5 Results

5.1 *Ultrasound Results*

Example results from the ultrasound measurements toward the lungs of the subjects are shown in Fig. 4. The measurements performed should indicate the thickness of the tissue that the light has to penetrate in order to reach gas. Although it is quite difficult to get exact measures of the depth since the placement of the probe is critical, the results indicated that the lung tissue (not necessarily gas), in this geometry, started at depths of 1.15, 1.53, and 1.03 cm for subjects 1, 2, and 3, respectively.

Gas-filled regions were found in the intestine in some of the ultrasound investigations performed on subjects 1 and 2, while no such clear findings could be seen for subject 3. Figure 5 shows one example of an ultrasound image of the intestine on each of the three subjects, down to a depth of ~2 cm. As seen, the gas pockets found for subjects 1 and 2 are located at depths of ~1 to 2 cm.

5.2 *Lung Spectroscopic Results*

For most laser/detector geometries, the light intensity received by the detector was extremely small due to the thick tissue. Further, in most positions, where the light transmission was reasonable, no absorption signal could be seen, since the light did not probe sufficiently deep to reach the gas in the lungs. However, in one position, as described in Fig. 3(a), it was possible to obtain WMS absorption signals by water vapor that was clear enough to distinguish with certainty for all subjects. The $2f$-demodulations of these absorption signals are presented in Fig. 6.

5.3 *Intestine Spectroscopic Results*

A variety of configurations in the positioning of the fiber tip and detector were tested in searching for gas imprints from the intestines. We found that, for subject 1, most positions did not give gas signals, neither for oxygen nor for water vapor. However, a couple of geometries were found where clear signals by water vapor were seen. Gas-filled cavities in the intestine had therefore been found. As a special case study, the signal strength was evaluated at four different fiber-to-detector separations. The results are presented in Fig. 7. The equivalent path-lengths presented indicate the average physical length that the light has passed through gas in the body.

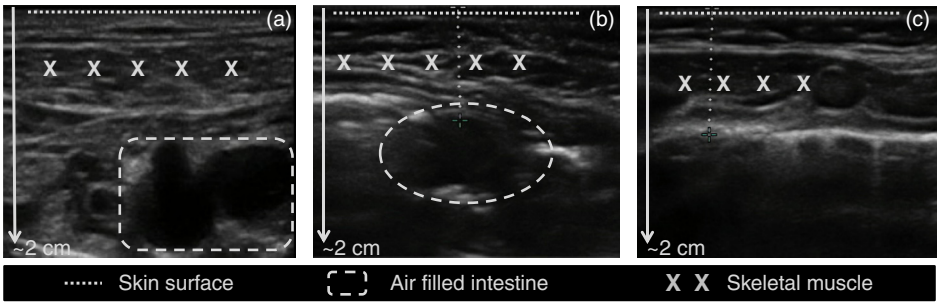

Fig. 5 Ultrasound images showing an abdominal cross-section of the three infants [(a) to (c), corresponding to subjects 1 to 3], ~2 cm of depth. The ultrasound probe was placed adjacent to the umbilicus. Skin surface, skeletal muscle, and air-filled intestine are indicated in the figures. In one of the images (c), due to normal bowel movements, a cross-section of air-filled intestine was not possible to capture.

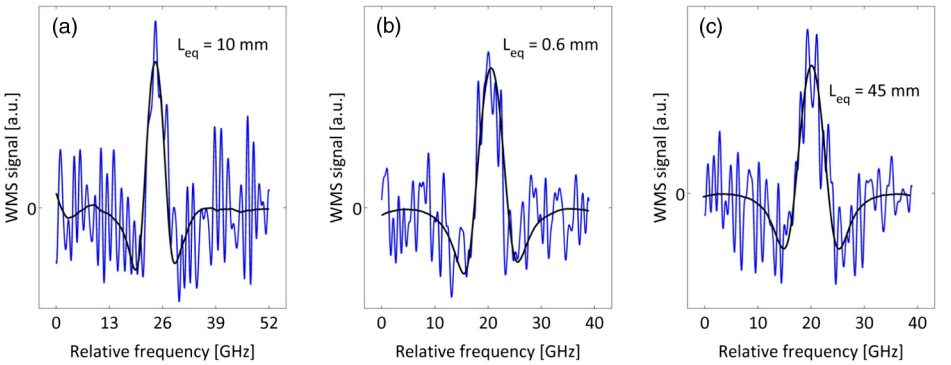

Fig. 6 Second harmonic demodulation of signal received with the light sent in just below the collar bone and detected below the armpit, as illustrated in Fig. 3(a). The figure shows the *in situ* signals (noisy) with fitted reference recordings (no noise). The SNR is low but enough to ensure contact with gas. Signal (a) is obtained from a measurement on subject 1, with an integration time of 60 s, (b) is from a measurement on subject 2, with an integration time of 40 s, and (c) is from subject 3, with an integration time of 60 s. The SNR is about the same in all recordings, even though the resulting L_{eq} values are very different, which can be ascribed to the fact that the received light intensity was much lower in the case of subjects 1 and 3, than in subject 2. The much smaller absorption signal received for subject 2 could still reach the same SNR as that of the others.

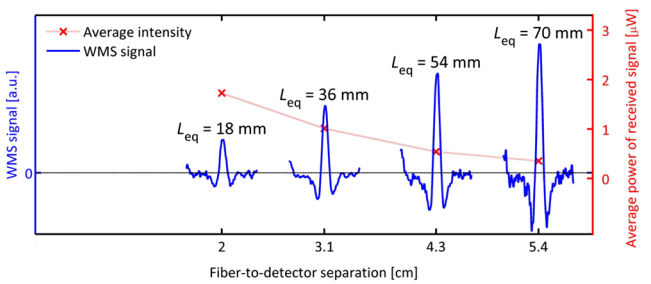

Fig. 7 Water vapor absorption (second harmonic WMS) signals and average received intensity obtained on the abdomen (geometry "b") with four fiber-to-detector separations. It is clearly shown how the absorption signal is increasing with increased separation, while the intensity is decreasing. The origin to these effects is shown in Fig. 9. The curves were each obtained from data obtained during 30 s.

For subject 2, water vapor absorption signals were found, both in the same geometry as for subject 1, i.e., with the fiber tip and detector placed on the stomach [Fig. 3(b), geometry b], and also with the fiber and detector placed on the lower part of the back [Fig. 3(c), geometry c]. For subject 3, intestinal gas signals were only received in geometry b. Figure 8 presents example results obtained in geometries b and c for subject 2, and in geometry b for subject 3.

As seen in Fig. 7, the acquired absorption signals by water vapor were strong and easily distinguished. The dependence on fiber-detector separation for the light intensity and absorption signal strength is further illustrated in Fig. 9. The origin of this effect is partly due to the fact that the light must travel a longer distance through tissue and probably also gas to reach the detector, and partly because a larger separation increases the probed depth into the tissue. The increased depth provides an increased probability of light reaching into the intestine. This separation-dependent penetration depth is shown with the help of results obtained by Monte Carlo simulations together with the

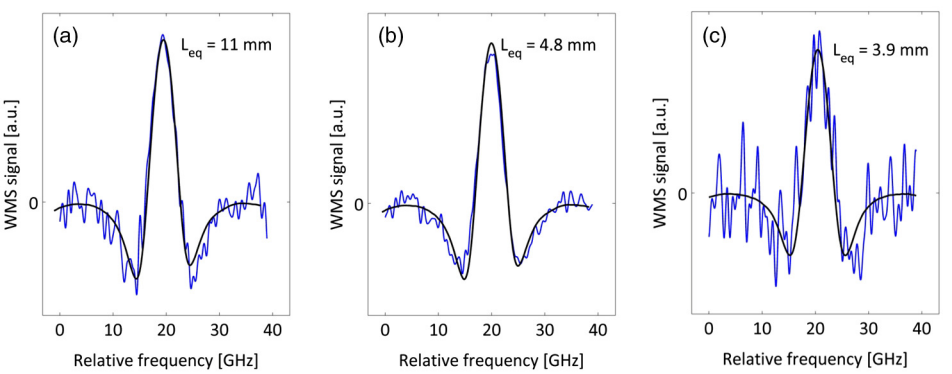

Fig. 8 WMS signals obtained on the intestine of subjects 2 and 3. The data in (a) is recorded on subject 2 in geometry "b" according to Fig. 3, (b) is recorded in geometry "c" on the same subject, and (c) is obtained from a recording in geometry "b" on subject 3. All recordings were done with an effective integration time of 10 s. Again, the SNR is not only related to the L_{eq}-value, but also to the received intensity, etc. As previously mentioned, the traces without noise show the fitted reference recordings.

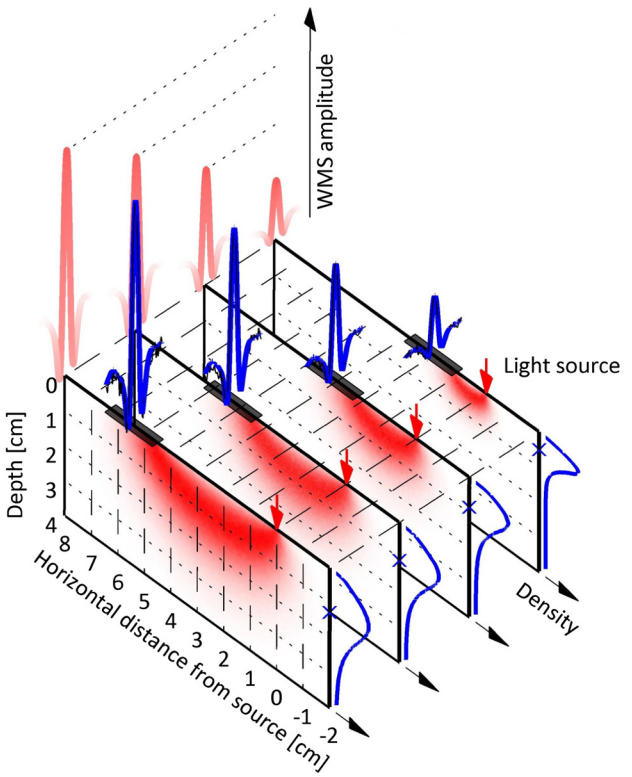

Fig. 9 Photon hitting density results from a Monte Carlo simulation of light injected into the tissue at one point and detected a certain distance away with an extended detector area. The profiles shown indicate the probability distribution of where the light that reached the detector went, on its way, from fiber to detector. As the distance between the detector and fiber is increased, the light probes deeper into the tissue (the detected light intensity is also rapidly decreasing). The density profiles shown to the right indicate the depth profile of the light penetration at the center plane between the fiber and detector and the cross indicates the average light depth at that plane. The gas absorption signals, or WMS signals, are thus increased with fiber-to-detector separation. Projections of the WMS signals are provided in the back plane for clearer intercomparison.

same experimental data as shown in Fig. 7. The figure shows the distribution of the conditional light injected through the fiber and detected by the detector. (Note that light that is emitted by the fiber tip is scattered in all directions with equal probability, while the presented profiles are only considering light that actually reaches the detector.) The parameters used in the simulations were $\mu_s' = 10\ \text{cm}^{-1}$ and $\mu_a = 0.25\ \text{cm}^{-1}$.

6 Discussion and Conclusions

In the present study, we have, for the first time, shown that a laser spectroscopic method could detect gas in the lungs and gastrointestinal tract of newborn human infants. The infants in this study were heavier and had greater tissue thicknesses than preterm infants, the subject population targeted for further studies. Despite this, signals were obtained from the lungs, even though these signals were of low quality, while high-quality water vapor signals were obtained in the intestinal measurements. We anticipate that localizing gas in the lungs and gastrointestinal tracts of very small infants should be possible based on the present results and the experience on how signals scale with thickness gained, e.g., from previous phantom studies.[13] Absorption signals were possible to detect for water vapor in the lungs, but not for oxygen, even if oxygen was definitely present in the lungs during the study. In a condition with 18% oxygen (approximate concentration in a lung) and 6.2% water vapor (saturated humidity at 37°C), the absorption of the latter is about ten times stronger. As the signal-to-noise ratios obtained for the water vapor signals in the lungs were in the order of 2 to 3, it is thus not surprising that oxygen was not observed. The results in Ref. 13, however, show how the signal quality is drastically increased when the thickness of the tissue surrounding the lungs is decreased. With the much thinner tissue of premature infants, a higher light intensity would be received, and a larger fraction of the light will have passed through gas; together these two effects should enable good absorption signals for both water vapor and oxygen. Both gases are important to probe. The water vapor signal is related to the total size of the cavity and provides a means to calibrate the oxygen signal. The amount and distribution of oxygen is dependent on the administered oxygen concentration in inspired air.

Water vapor is always present in human cavities, and spectroscopic detection of this gas for gas pocket assessment might prove competitive over, e.g., ultrasound, also in the case of nonspecific gas detection. Reasons for this are, for example, that the spectroscopic method requires little computing power and quite simple equipment. Moreover, the personnel handling of the equipment does not need much training in its use.

Preterm infants in need of ventilatory support are monitored with oxygen saturation and intermittent arterial and venous blood gases as well as chest x rays, the latter usually performed only a few times with relatively long time intervals. The addition of a new noninvasive method to immediately and repeatedly assess the effect of changes in the ventilation would highly improve precision of care. Rapid bed-side detection of free gases outside the lungs and intestines would be an important achievement resulting in fewer complications. The technique presented here has the potential to be developed for continuous monitoring of gas distribution inside and outside the lungs. Further, it may be useful as an additional tool in the diagnosis of NEC and other disorders with changes in gas distribution in tissue.

Further investigations are planned to be performed at Skåne University Hospital, Lund, Sweden.

Acknowledgments

This work was supported by the Swedish Research Council through a direct grant and through a Linnaeus grant to the Lund Laser Centre, and through the Lund University Medical Faculty. Valuable inputs to the manuscript were given by Dr. Lars Björklund. The authors would like to thank the three infants for friendly collaboration during measurements.

References

1. R. L. Goldenberg et al. "Epidemiology and causes of preterm birth," *Lancet* **371**(9606), 75–84 (2008).
2. D. G. Sweet et al., "European consensus guidelines on the management of neonatal respiratory distress syndrome in preterm infants—2013 update," *Neonatology* **103**(4), 353–368 (2013).
3. A. Greenough, A. D. Milner, and G. Dimitriou, "Synchronized mechanical ventilation for respiratory support in newborn infants (cochrane review)," *Cochrane Database Syst. Rev.* **2001**(1), CD000456 (2001).
4. J. Pietz et al., "Prevention of necrotitizing enterocolitis in preterm infants: a 20-year experience," *Pediatrics* **119**(1), 164–170 (2007).

5. M. Veenendaal et al., "Effect of closed endotracheal suction in high-frequency ventilated premature infants measured with electrical impedance tomography," *Intensive Care Med.* **35**(12), 2130–2134 (2009).
6. M. Lewander et al., "Non-intrusive gas monitoring in neonatal lungs using diode laser spectroscopy: feasibility study," *J. Biomed. Opt.* **16**(12), 127002 (2011).
7. S. Svanberg, "Optical analysis of trapped gas—gas in scattering media absorption spectroscopy," *Laser Phys.* **20**(1), 68–77 (2010).
8. P. Lundin et al., "Non-invasive gas monitoring in newborn infants using diode laser absorption spectroscopy: a case study," *Proc. SPIE* **8229**, 822903 (2012).
9. L. O. Svaasand, T. Boerslid, and M. Oeveraasen, "Thermal and optical properties of living tissue: application to laser-induced hyperthermia," *Laser Surg. Med.* **5**(6), 589–602 (1985).
10. J. Parrish, "New concepts in therapeutic photomedicine: photochemistry, optical targeting and the therapeutic window," *J. Invest. Dermatol.* **77**(1), 45–50 (1981).
11. J. Boulnois, "Photophysical processes in recent medical laser developments: a review," *Lasers Med. Sci.* **1**(1), 47–66 (1986).
12. L. Persson et al., "Gas monitoring in human sinuses using tunable diode laser spectroscopy," *J. Biomed. Opt.* **12**(5), 054001 (2007).
13. L. Persson et al., "Non-intrusive optical study of gas and its exchange in human maxillary sinuses," *Proc. SPIE* **6628**, 662804 (2007).
14. M. Lewander et al., "Clinical system for non-invasive in situ monitoring of gases in the human paranasal sinuses," *Opt. Express* **17**(13), 10849–10863 (2009).
15. M. Lewander et al., "Non-invasive diagnostics of the maxillary and frontal sinuses based on diode laser gas spectroscopy," *Rhinology* **50**(1), 26–32 (2012).
16. S. Lindberg et al., "Method for studying gas composition in the human mastoid cavity by use of laser spectroscopy," *Ann. Otol. Rhinol. Laryngol.* **121**(4), 217–223 (2012).
17. J. Alnis et al., "Laser spectroscopy of free molecular oxygen dispersed in wood materials," *Appl. Phys. B* **77**(6), 691–695 (2003).
18. T. Svensson et al., "Noninvasive characterization of pharmaceutical solids by diode laser oxygen spectroscopy," *Appl. Spectrosc.* **61**(7), 784–786 (2007).
19. T. Svensson et al., "VCSEL-based oxygen spectroscopy for structural analysis of pharmaceutical solids," *Appl. Phys. B* **90**(2), 345–354 (2008).
20. T. Svensson and Z. Shen, "Laser spectroscopy of gas confined in nanoporous materials," *Appl. Phys. Lett.* **96**(2), 021107 (2010).
21. M. Lewander et al., "Food monitoring based on diode laser gas spectroscopy," *Appl. Phys. B* **93**(2–3), 619–625 (2008).
22. M. Lewander et al., "Non-intrusive measurements of headspace gas composition in liquid food packages made of translucent materials," *Packag. Technol. Sci.* **24**(5), 271–280 (2011).
23. L. Persson et al., "Diode laser absorption spectroscopy for studies of gas exchange in fruits," *Opt. Laser Eng.* **44**(7), 687–698 (2006).
24. U. Tylewicz et al., "Gas in scattering media absorption spectroscopy (GASMAS) detected persistent vacuum in apple tissue after vacuum impregnation," *Food Biophys.* **7**(1), 28–34 (2012).
25. M. Andersson et al., "Flexible lock-in detection system based on synchronized computer plug-in boards applied in sensitive gas spectroscopy," *Rev. Sci. Instrum.* **78**(11), 113107 (2007).
26. B. C. Wilson and G. Adam, "A Monte Carlo model for the absorption and flux distributions of light in tissue," *Med. Phys.* **10**(6), 824–830 (1983).
27. L. H. Wang, S. L. Jacques, and L. Q. Zheng, "MCML—Monte Carlo modeling of light transport in multi layered tissues," *Comput. Methods Programs Biomed.* **47**(2), 131–146 (1995).
28. E. Alerstam, S. Andersson-Engels, and T. Svensson, "White Monte Carlo for time-resolved photon migration," *J. Biomed. Opt.* **13**(4), 041304 (2008).

Biographies of the authors are not available.